Novel algorithms for efficiently accumulating, analysing and visualising full-waveform LiDAR in a volumetric representation with applications to forestry

submitted by

Milto Miltiadou

for the degree of Doctor of Engineering

of the

University of Bath

Centre for Digital Entertainment

and of the

Plymouth Marine Laboratory

NERC Airborne Research Facility

April 2017

Chapter 1

Introduction

1.1 Forest Monitoring: Importance and Applications

Forest monitoring involves checking and observing the changes in the structure of the forests and their foliage over the years. It has a significant value in both sustainable and commercial forests, because it contributes to managing biodiversity, maintaining forest health and optimising wood trade procedures as explained below:

- **Biodiversity** plays a substantial role in ecosystem resilience [1] while various human activities affect biological communities by altering their composition and leading species to extinction [2]. For example, in Australian native forests many arboreal mammals and birds rely on hollow trees for shelters [3] . Hollow trees are trees that have hollows, which are semi-enclosed cavities on trunks and branches. They are formed by natural forces, like bacteria, fungi and insects and may take tens to hundreds of years to become suitable for animal/bird shelters. Unfortunately recent studies shown that there us likely to be a shortage of hollows available for colonisation in the near future [4] [5]. Therefore monitoring and protecting hollow trees has a positive impact in preserving biodiversity.

- **Forest Health**: Protecting vegetation from pests and diseases. An example of pests are the Brushtail Possums, which were initially brought to New Zealand for fur trade, but they have escaped and become a thread to native forests and vegetation [6]. In addition, anthropogenic factors have a negative impact to nature. For instance, acid rain is responsible for the freezing decease at red bruces because it reduces the membrane-associated calcium, which is important for tolerating cold [7]. Those changes in nature need to be monitor in order to preserve a healthy and resilience ecosystem.

- **Wood Trade**: Measuring stem volume and basal areas of trees contributes to forest planning and management [8]. For example, measuring stocking and wood quality would help into estimating the cost of harvesting the trees in relation to the stocking [9].

Traditionally, forest monitoring involves field work such as travelling into the area of interest and taking manual measurements. Regarding the need to monitor hollows, tree climbing with ladders and ropes gives very accurate results but is dangerous, expensive, time consuming, and cannot easily scale into surveying large forested areas [10] [11]. Therefore, automated ways of monitoring forests are essential and this is why Remote Sensing has a significantly positive impact in forestry.

1.2 Background Information about Remote Sensing and Airborne Laser Scanning Systems

Remote sensing refers to the acquisition of information about objects, for example vegetation and archaeological monuments, without physical contact and the subsequent interpretation of that information. The sensors used to capture the information are divided into passive and active. For example satellite photography is passive because information are collected from the reflected natural sun light, while Airborne Laser Scanners (ALS) are active because they emit laser beams and collects information from the backscattered laser energy [12].

According to Wanger et al, Airborne Laser Scanning (ALS) is a growing technology used in environmental research to collect information about the Earth, such as vegetation and tree species. Comparing ALS with traditional photography, ALS is not influenced by light and it is therefore less dependent on weather conditions (ie. it collects information from below the clouds, or at night). The laser beam also partially penetrates the tree canopies allowing it to record information about the forest structure below the canopy, as well as the ground [13]. ALS methods are divided into pulse systems, which repeatedly emit pulses, and continuous wavelength systems that continuously emit light. They both acquire information from the backscattered laser intensity over time, but continuous wavelength systems are more complicated because they obtain one extra physical parameter, the frequency of the ranging signal. Further, according to Wehr and Lohr, continuous wavelength systems are 85 times less accurate than pulse systems [14].

LiDAR (Light Detection And Ranging) systems are active and pulse laser scanning systems [14]. They are divided into two groups according to the diameter of the footprint left by the laser beam on the ground, which is primarily dependent on the distance between the sensor and the target (altitude, in most remote sensing) and the beam divergence. The small-footprint group has a 0.2-3m diameter, is widely commercialised and the sensors are mostly carried on planes (ALS systems). In contrast, the large-footprint systems have a wider diameter (10-70m) and during experiments they were mostly mounted on satellites. Small-footprint systems record at higher resolution but cannot guarantee that every pulse will reach the ground due to the small diameter of their footprint, making topographic measurements difficult, and are limited to smaller survey areas due to the cost and availability of aircraft. In contrast, large-footprint scanners have wider diameters and can therefore scan wider areas with the likelihood of recording the ground to be higher [15] .

In addition, there are two types of LiDAR data: discrete and full-waveform (FW). Discrete LiDAR records a few peaks of the reflected laser intensity, while FW LiDAR stores the entire backscattered signal. The discrete LiDAR has been widely used and a 40% reduction of fieldwork has been achieved at Interpine Ltd Group, New Zealand, with that technology. Regarding the newer FW LiDAR, scientists understand their concepts and potentials but due to the shortage of available tools able to handle these large datasets, there are very few uses of FW LiDAR [16].

The design of the first FW LiDAR system was introduced in 1980s, but the first operational system was developed by NASA in 1999 [17]. The vastly increased amount of information recorded within the FW LiDAR suggests many new possibilities and problems from the point of view of image understanding, remote surveying and visualisation. As an indication, a 9.3GB discrete LiDAR from New Forest, UK, corresponds to 55.7GB of FW LiDAR.

This research is focused on the representation and efficient use of FW LiDAR data and contributes both to forestry visualisations and classifications. Two datasets are used for testing and evaluation: the New Forest and the RedGum dataset. An in-depth explanation of LiDAR systems and the specifications, differences and challenges of the two datasets are given in Section 2. An overview of the specific aims, objectives and contributions of this thesis, set in the context of these datasets, is then given at Section 3.

Chapter 2

Acquire Data

The aim of this section is to give a practical and scientific insight into the acquisition of data, because a good knowledge of these methods and their limitations is essential for understanding the related research undertaken. The relations between the two main datasets used in this project are depicted on Figure 2-1 and briefly explained here:

- The **New Forest dataset** from the UK was provided by the Natural Environment Research Council's Airborne Research Facility (NERC ARF). Measurements were collected simultaneously a Leica ALS50-II LIDAR and AISA Eagle/Hawk hyperspectral radiometers on the 8th of April in 2010. It contains Discrete LiDAR, FW LiDAR and hyperspectral images.

- The **RedGum dataset** was acquired in Australia using a Trimble AX60 integrated LIDAR/Camera instrument over the time period from the 6th of March in 2015 until the 31st of March in 2015. It was provided by the RPS Australia East Pty Ltd. Only the FW LiDAR data are used here.

The ALS data are explained first, because they are the main focus of this research, and hyperspectral imagery is towards the end of the chapter. In Section 2.1, an in-depth description of ALS systems and the differences between discrete and FW LiDAR data is given. Section 2.2 briefly discusses the binary file format of the acquired LiDAR data and Section 2.3 is a discussion on the limitations, the differences and the advantages of two LiDAR instruments; the Leica and Trimble. The essential information about the hyperspectral imagery, which is only associated with the New Forest dataset, is then covered in Section 2.4.

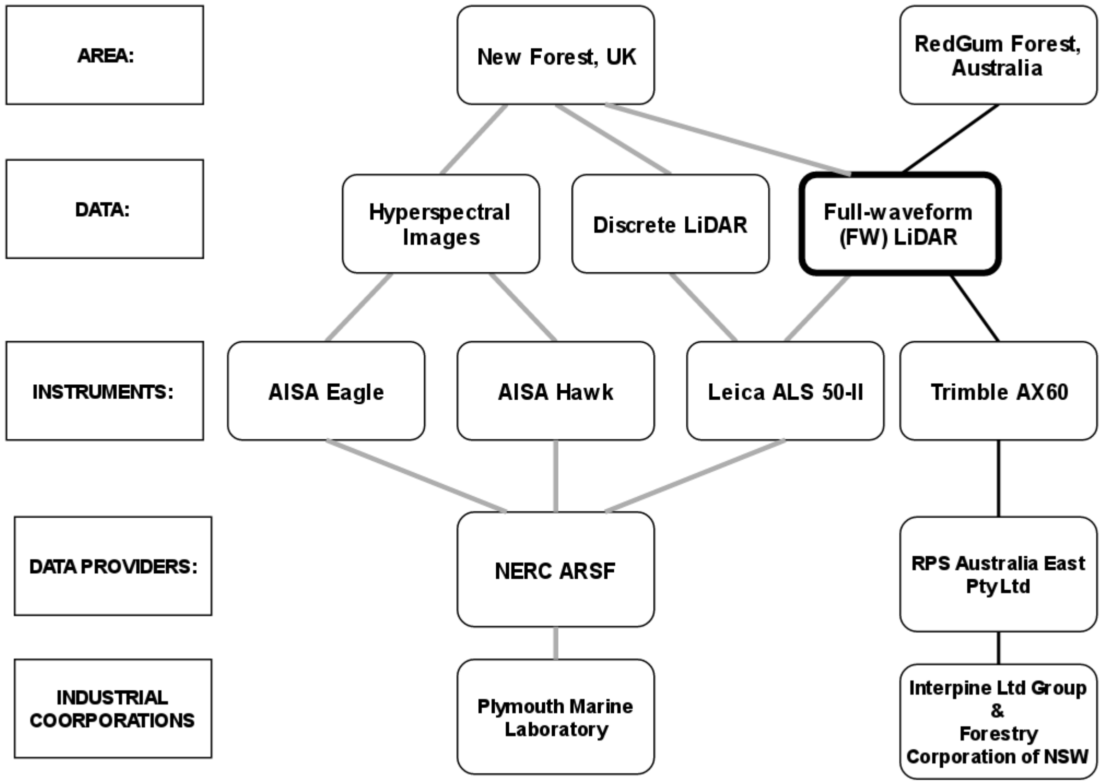

Figure 2-1: Data and Instruments

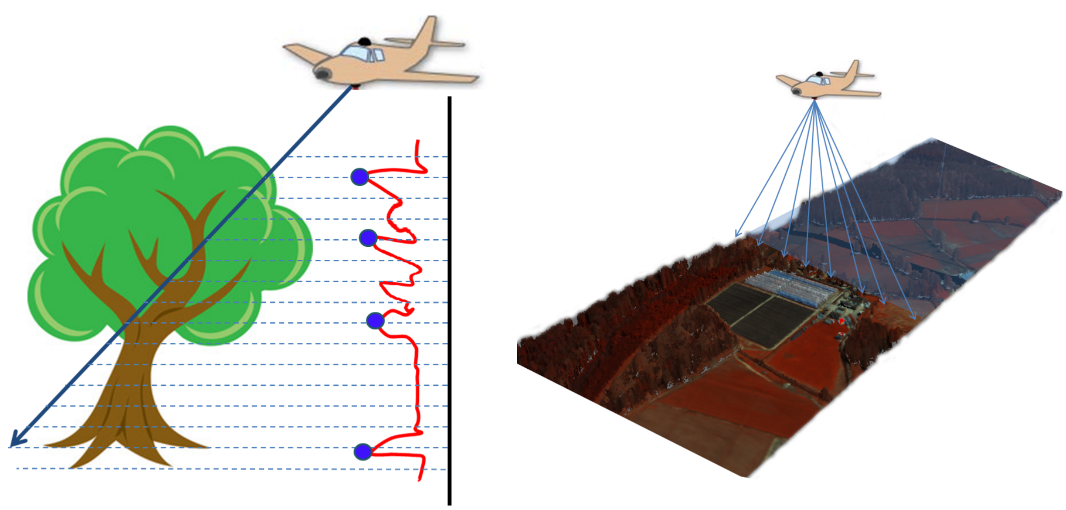

(a) A Pulse: Discrete Vs Full-Waveform (b) A Flightline

Figure 2-2: Airborne Laser Scanning System

2.1 Airborne LiDAR systems: An in-depth Explanation

The ALS systems emit laser pulses from sensor mounted in a plane and collects information from the time-of-flight and the returned laser intensity. By the time the pulse has travelled the approximately 1-3km from the aircraft to the ground, it is roughly 20cm in width due to beam divergence. When the pulse hits an object (e.g. the forest canopy), then some of it reflects back while the rest penetrates through holes between leaves and branches. The laser pulse continues to hit structures, scattering and partially returning to the sensor until it reaches a solid barrier such as the ground and is fully blocked from further progress. The LiDAR systems record information from the backscattered laser pulse, measuring its round trip time and the returned intensity.

As mentioned at Section 1.2, there are two types of LiDAR data, discrete and FW. The discrete LiDAR observes the returned intensity signals and identifies and records a few peak intensity returns of the signal, while the FW LiDAR system digitises and stores the enitre backscattered signal into equally spaced time intervals (Figure 2-2a). The delivered data for the discrete LiDAR is a set of hit points ("returns"), which are associated with laser intensities. The world position of every return is calculated by measuring the round trip time of the laser return, giving a distance from the sensor, which is combined with the precisely known position and orientation of the aircraft/sensor (from GPS, an inertial measurement unit and precise shot direction of the laser pulse). The waveform recordings are triggered by and attached to first returns of discrete LiDAR data (to avoid sampling the uninteresting time period while the pulse travels through the atmosphere) and they are a list of intensities that correspond to the laser intensity returned over time. There is also an offset vector which defines the distance and direction between each wave sample (effectively a compression mechanism, by avoid recording the world position of every sample, replacing it with the location of the first return and this vector).

As shown in Figure 2-2b, the pulses are scanned back and forth across the landscape below (by a rotating mirror) as the plane travels forward. The scanned data has a limited maximum width according to the flight height and the field of view scan angle. During processing the track of the plane is divided into easier-to-handle pieces (flightlines) and saved into separate binary files. In this project the LAS1.3 file format is used for both datasets.

2.2 Brief Description of the LAS1.3 File Format

There are a few LiDAR file formats but the LAS1.3 was the first format to contain FW data and it is the one used to store the data for both New Forest and RedGum datasets. According to the LAS1.3 file specifications [18], a .LAS file contains information about both discrete and FW LiDAR data, with the waveform packets are attached to discrete returns and saved either internally at the end of the .LAS file or externally in a .WVS file.

As shown at (Figure 2-3) the .LAS file is divided into four sections and a brief explanation of each section is given here:

1. The **Header** contains general information about the entire flightline. For example, it includes the maximum scan angle used during the flight, whether the waveform packets are recorded internally or externally and the number of **Variable Length Records** (VLR).

2. Regarding the **VLR**, which contain arbitrary "extension" data blocks, the most important information given is the waveform packet descriptors that contain essential information on how to read the waveform packets (i.e. an ID, the number of wave samples and the size of each intensity in bits).

3. The **Point Data Records** are the discrete points and the waveforms are associated with first return discrete points. Each Point Data Record has a spatial location, an intensity and optionally a pointer to a waveform packet as well as the ID of the corresponding waveform packet descriptor.

4. The waveform packets is a list of intensities and they are either saved internally into the **Extended Variable Length Records** section of the .LAS file or inside an external .WVS file. Starting from the associated first return point, the spatial locations of the waveform packet (wave sample intensity) are calculated by adding an offset defined in the associated Point Data Record.

2.3 Leica Vs Trimble Instruments: Limitations, Differences and Advantages

As shown in Figure 2-1, the Leica ALS 50-II instrument was used to capture the LiDAR data of New Forest dataset and the Trimble AX60 for collecting the RedGum Forest FW LiDAR data. It is therefore important to clarify the differences, the limitations and the advantages of each instrument.

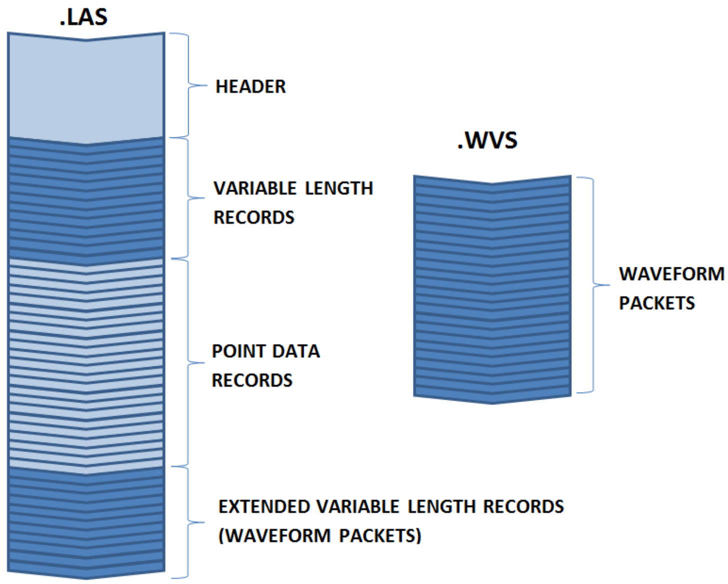

Figure 2-3: How the FW LiDAR data are stored into a binary file, according to the LAS1.3 file format specification

The Trimble performs at a pulse frequency of 400kHz, while the Leica's maximum pulse frequency is 120kHz. Nevertheless, during experiments there were occasions when the Leica discarded every other waveform due to I/O limitations despite being at or below the maximum pulse frequency [19]. The New Forest dataset has been affected by this and, on average, one third of the saved pulses only contain discrete data. We should therefore be extremely careful when comparing Discrete with FW LiDAR data. While [16] concludes that FW LiDAR data worth the extra processing because they have a better vertical profile, [20] states that extra information (the echo-width) from the FW LiDAR data are relatively unimportant. But the New Forest datasets were used for the comparison at [20] and there is no mention about the significantly less waveforms recorded in comparison to the discrete data. It is therefore suspected that their results has been affected by the missing waveforms.

Another problem with the Leica sysyem is the small dynamic range of intensities due to the number of bits used for recording them; the Leica system uses 8-bit integers (0-255 range) while the Trimble uses 16-bit integers (0-16385 range). For increased dynamic range and finer intensities without doubling storage costs, Leica introduced an Automatic Gain Controller (AGC). The AGC is an 8-bit number that defines how the recorded intensity range is shifted across a wider range of intensities. The AGC value is adjusted according to the reflected laser intensity of the previous 64 pulses and it therefore varies across a flightline. Consequently, the raw intensities are incomparable to each other and, since the relation between AGC and the intensities is not linear, the range normalisation is complicated [21] [22]. In this thesis, the intensities of the Leica system are used as boolean values (whether something existed or not, using a user-defined threshold) to quickly overcome that issue and focus on the major research objectives. Regarding the Trimble instrument, there is no AGC value because the intensities are saved into a 16bit integer and as long as the flight height is constant no normalisation is required. In a few words, the raw intensities recorded using the Leica system are not normalised and therefore not comparable to each other, while the intensities of the Trimble instrument are more meaningful.

The footprint of the laser on the ground depends on the scanning pattern of the instruments and the field of view. The sinusoidal scanning pattern of the Leica system results in a higher density of returns at the edges of the flightline. The footprint of the Trimble instrument is more equally spaced because they are scanned using a rotating polygon. The uneven density pattern of the Leica system is resolved by normalisation during the voxelisation process, but the Trimble's equally spaced pulse pattern is more prone to aliasing when voxelised. Regarding the field of view, the Leica is wider but both systems avoid large angles because otherwise data look deformed at edges of the flightlines.

Last but not least, the Trimble instrument is a native full-waveform sensor; the discrete LiDAR are produced by extracting peak points in post-processing. Therefore one of the purported advantages of a FW system, the concept of extracting a denser point clouds using Gaussian decomposition [13], does not apply in the Trimble's case. This was proven by extracting peak points from Trimble FW LiDAR data using the pulseextract from LAStools [23]; the number of points extracted was exactly the same as the number of points saved into the associated discrete LiDAR files. Therefore discrete data from the Trimble instrument are the same as those generated by echo decomposition and peak points extraction from the FW samples.

To sum up, the Trimble AX60 instrument is a newer sensor and therefore has less problems or design compromises in comparison to the Leica ALS50-II instrument. Table 2.1 summarises the differences between the two sensors.

2.4 Hyperspectral Imagery

Hyperspectral imagery has a positive impact in remote sensing because it contains information beyond human visibility. The human eye receives light from the visual spectrum into three bands (red, green and blue). The hyperspectral sensors captures a larger spectrum and divides its light components into hundreds of bands, recording

Table 2.1: Specifications of the LiDAR instruments used

Instrument Name:	Leica ALS550-II	Trimble Ax60
Scanned Area	New Forest, UK	RedGum, Australia
Year of Introduction:	Discrete LiDAR 2009 & FW LiDAR 2010	2013
Max Scan Frequency (kHz):	120	400
Recorded Intensity (bits):	8	16
AGC:	Yes	No
Scanning Pattern:	Sinusoidal	The footprints are more equally spaced on the ground
Max field of view (degrees):	75	60

this way more information than a human eye can receive [12].

Nevertheless, there are other compromises - for example, the time taken to integrate incoming light as the aircraft carrying the sensors moves. This means the raw airborne images appear deformed because the pixel length varies across the flightline. NERC-ARF geo-corrects the data using the Airborne Processing Library (APL) [24]. The processing levels are numbered. At 'level 3' (world coordinate system) the pixels are equally spaced and sized, which requires resampling and thus may look slightly blurred. The 'level 1' data (what the sensor saw) are non geo-corrected but they are associated with a file that defines the spatial location of each pixel. In this thesis, the 'level 1' data are used to preserve the highest possible quality.

In practise, the level 1 data are held in two files, the '.bil' and the '.igm'. The '.bil' file contains the hyperpsectral cube (Figure 2-4), all the pixel values at different wavelengths, and the .igm file gives the x, y, z coordinates of each pixel.

The number of bands and the spectrum range captured depends on the hyperspectral sensor. The data from New Forest were collected using the following instruments:

- the Eagle, which captures the visible and near infra-red spectrum (400-970nm)
- the Hawk, which covers short wave infra-red wavelengths (970-2450nm)

Both sensors divide their spectral range into 252 bands (programmable) and each band is a 2D vector as shown in Figure 2-4).

The hyperspectral images also come with a number of drawbacks. A few are mentioned here but since hyperpsectral imagery is not the main focused of the thesis there are not addressed:

- System faults sometimes occurs and the affected areas are masked out. This results in blank areas.

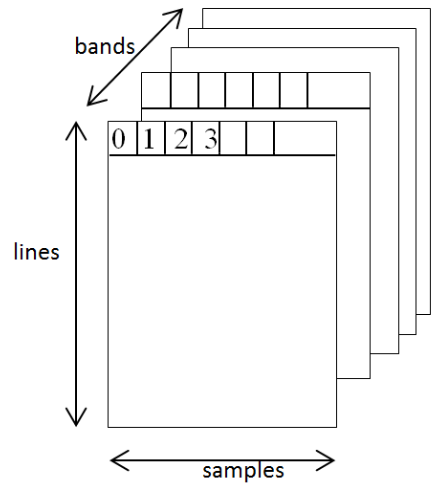

Figure 2-4: This figure shows the order of the hyperspectral pixels saved into the the binary .bil file.

- As a passive sensor, it is dependent on the sun for illumination and thus vulnerable to poor weather conditions

- Due to the high refraction of light at some wavelengths, some bands are highly influenced by humidity (i.e. wavelength 1898.33nm).

To sum up, hyperpsectral images contain information beyond the visible and they are delivered in two files, one contains the hyperspectral cube and the other one the geo-locations of each pixel. In this project, they are used in chapter (Chapter 7), where it is shown that the combination of Remote Sensing data confers better results for generating tree coverage maps.

Chapter 3

Overview of Thesis

3.1 Problem

FW LiDAR systems have been available for a number of years but there still very few uses of FW LiDAR data. NERC-ARF has been acquiring airborne data for the UK and overseas since 2010 and it has more than 100 clients of new and archived data. Many clients request FW LiDAR data to be acquired, but despite the significant number of requests,the majority of research still only uses discrete LIDAR. Some of the factors regarding this slow intakes are:

- Typically FW datasets are 5 – 10 times larger than discrete data, with data sizes in the range of 50GB – 2.5TB GB for a single area of interest. NERC-ARF's datasets are up to 100GB each because most clients are research institutes but for commercial purposes each FW dataset is a couple of TB.

- Existing workflows are only able to work with the discrete data since the increased amount of information recorded within the FW LiDAR makes handling the quantity of data very challenging.

Chapter 4

The open source software DASOS and the Voxelisation Approach

As mentioned in Section 3.1, there are very few uses of FW LiDAR data because of the quantity of the recorded information. For that reason, DASOS was developed (Section 4.3) as an open source software, to help foresters without computer science background to use FW LiDAR data while simultaneously advancing the research goals of this thesis. In this section:

- An overview of related software packages is given and we explain how DASOS differs from those packages (Section 4.1).
- The main method of interpreting the data within DASOS (the voxelisation approach) is described (Subsection 4.2).
- All the functionalities of DASOS are listed (Section 4.3)
- and, finally, a summary is provided (Section 4.4).

4.1 State-of-Art FW LiDAR Software Packages

The most common approach for interpreting FW LiDAR is the Gaussian decomposition of the waveforms for peak-points extraction. Each waveform is modelled as a set of Gaussian pulses and for every Gaussian peak, a single return (equivalent to a discrete LiDAR point) is extracted [28]. Neunschwander et al used this approach for Landcover classification [29] while Reitberger et al applied it for distinguishing deciduous trees from coniferous trees [30]. Chauve et al further proposed an approach of improving the Gaussian model in order to increase the density of the points extracted from the data and consequently improve point based classifications of FW LiDAR data [17]. The following tools are able to extract discrete points from the waveforms and visualise small areas of interest:

- **Pulsewaves**: visualises a small number of waveforms using different transparencies according to the intensities of the wave-samples and is able to generate discrete point clouds [25].
  Link: `<https://rapidlasso.com/pulsewaves/>`
- **FullAnalyze**: supports echo decomposition. Regarding visualisations, the user can select single trees from the Graphical User Interface (GUI) and, for each wave-sample, a sphere with radius proportional to its amplitude is created and visualised [31].
  Link: <http://fullanalyze.sourceforge.net/>
- **SPDlib**: exports discrete LiDAR and visualises either the samples that are above a threshold level as points or the extracted discrete point cloud. It also colours them according to their intensity value [32].
  Link: <http://www.spdlib.org/>

Echo decomposition and extraction of peak points identifies significant features and further enables the interpretation of the data within existing workflows and software that support discrete LiDAR data. For example, the discrete LiDAR can be analysed using:

- **Lag**: a visualisation tool for analysing and inspecting discrete LiDAR point clouds.
  Link: <http://arsf.github.io/lag/>
- **Quick Terrain Modeller** : a 3D discrete LiDAR points visualiser, that can generate Digital Elevation Models (DEM) and Digital Terrain Models (DTM).
  Link: <http://appliedimagery.com/>
- **LAStools** : a tool set that classifies noise, visualises point clouds, clips data.
  Link <https://rapidlasso.com/lastools/>

The DASOS approach to interpreting FW LiDAR data is fundamentally different from the aforementioned software packages. On the one hand, converting FW LiDAR into discrete peaks eases their usage, since existing workflows support discrete LiDAR. On the other hand, FW LiDAR contains information about pulse width that is not preserved after peak point extraction. Also the comparison of point clouds depends on the density of the emitted pulses; problems arise with the sinusoidal scannng pattern of, for example, the Leica system, resulting in higher numbers of samples at the edges of the swath and lower in the middle. For these reasons, in DASOS, this information is accumulated from multiple shots into a voxel array, building up a 3D density volume. The correlation between multiple pulses in a voxel representation produces a more accurate and complete representation, which confers greater noise resistance and it further opens up possibilities of vertical interpretation of the data. The idea of voxelising FW LiDAR data is explained in the following section 4.2.

4.2 Voxelisation for Interpreting FW LiDAR data

Voxelisation of FW LiDAR data was first introduced by Persson et al., who used it to visualise waveforms using different transparencies [26] and it has been adopted as the future of FW LiDAR data with the literature moving toward that direction. In 2016-17, Cao et al used it for tree species identification [33], Hancock et al improved canopy height models of vegetation [34] and Sunmall et al characterised forest canopy from a voxelised vertical profile [20]. The innovative approach of voxelising the FW LiDAR data is an integral part of this thesis and it is used for both visualisations and classifications [35] [27].

The FW LiDAR data are voxelised by inserting the wave samples into a 3D regular grid and constructing a 3D discrete density volume. According to Persson et al, each wave sample is associated with the 3D cell, named voxel, that it lies inside. If multiple samples lie inside a voxel then the sample with the highest intensity is chosen [26]. In order to reduce noise, there are two differences between this approach and the way FW LiDAR data are voxelised in DASOS.

At first a threshold is used to remove low level noise, because when the length of a recorded waveform is longer that the distance between the first hit point and the ground, the system captures low signals for the remaining sampling time period after the pulse has been absorbed by the ground, which results pure noise. For that reason, the samples whose intensity is lower than a user-defined noise level/threshold are discarded.

As before, each wave sample is associated with the voxel that it lies inside. The second difference is how DASOS overcomes the uneven number of samples per voxels, which is primarily caused by the differing angle at which the LiDAR shot passes through voxels directly below the sensor and those off to the sides. The intensity of each sample is the laser intensity returned during the corresponding time interval. For example, if 5 samples are inside a voxel and the waveform is digitised at 2ns, then the laser intensity associated with that voxel corresponds to a 10ns waveform sampling length. For comparison purposes, it's essential to keep the waveform length consistent across the voxels. To overcome this issue in DASOS, the average intensity of the samples that lie inside each voxel is taken, instead of choosing the one with the highest intensity [26]. This way, the likelihood that the 3D volume will be affected by outliers and high noise is reduced. The following equation shows how the intensity value of a voxel is calculated:

$$I_v = \frac{\sum_{i=1}^{n} I_i}{n} \tag{4.1}$$

where I_v is the accumulated intensity of voxel v, n is number of samples associated with that voxel and I_i is the intensity of the sample i.

To sum up, during voxelisation, the area of interest is divided into voxels. The samples of the FW LiDAR data are inserted inside this 3D discrete density volume and normalised such that equally sized waveform length is saved inside each voxel. The result is a 3D discrete density volume of the scanned area. Figure 4-1 depicts this process in 2D.

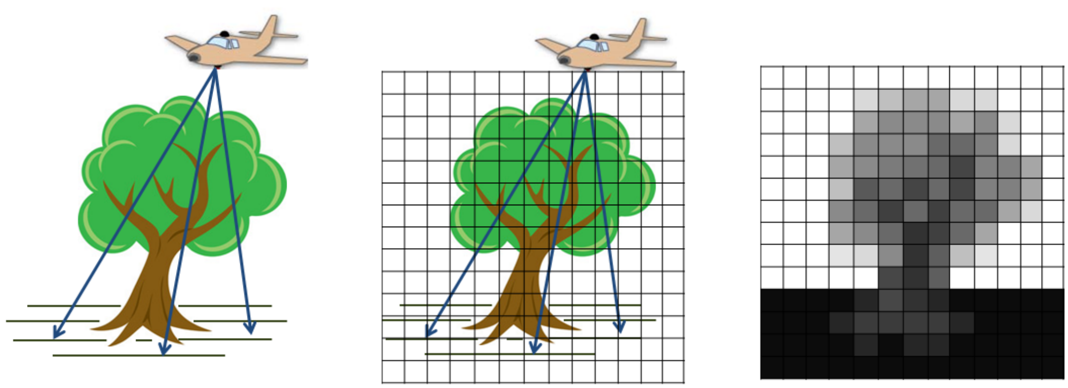

(a) The sensor from the plane emits multiple pulses and collects information from the returned laser intensity.

(b) The area of interest is divided into equally sized cubes, named voxels, generating this way a discrete volume.

(c) The accumulated intensities of wave samples into the volume build up the voxelised representation of the scanned area.

Figure 4-1: The above images depict the voxelisation process of the FW LiDAR data in 2D. Please note that the voxelisation output in Figure 4-1c shows how ideally the result would look. But in reality, a number of trees may be disconnected from the ground due to missing information about their trunk. [1]

[1] The tree and plane images are taken from: http://images.clipartpanda.com/tree-clip-artKij4jKriq.jpeg & http://gmv.cast.uark.edu/wpcontent/uploads/2013/01/ALS_scematic.jpg

Bibliography

[1] T. Elmqvist, C. Folke, M. Nyström, G. Peterson, J. Bengtsson, B. Walker, and J. Norberg, "Response diversity, ecosystem change, and resilience," *Frontiers in Ecology and the Environment*, vol. 1, no. 9, pp. 488–494, 2003.

[2] D. U. Hooper, F. S. Chapin Iii, J. J. Ewel, A. Hector, P. Inchausti, S. Lavorel, and B. Schmid, "Effects of biodiversity on ecosystem functioning: a consensus of current knowledge," *Ecological monographs*, vol. 75, no. 1, pp. 3–35, 2005.

[3] D. B. Lindenmayer and J. T. Wood, "Long-term patterns in the decay, collapse, and abundance of trees with hollows in the mountain ash (eucalyptus regnans) forests of victoria, southeastern australia," *Canadian Journal of Forest Research*, vol. 40, no. 1, pp. 48–54, 2010.

[4] R. L. Goldingay, "Characteristics of tree hollows used by australian birds and bats," *Wildlife Research*, vol. 36, no. 5, pp. 394–409, 2009.

[5] P. Gibbons and D. Lindenmayer, *Tree Hollows and Wildlife Conservation in Australia*. CSIRO Publishing, 2002.

[6] "Animal pests: Poss." http://www.doc.govt.nz/conservation/threats-and-impacts/animal-pests/animal-pests-a-z/possums/. Accessed: 19th of September 2014.

[7] D. H. DeHayes, P. G. Schaberg, G. J. Hawley, and G. R. Strimbeck, "Acid rain impacts on calcium nutrition and forest health alteration of membrane-associated calcium leads to membrane destabilization and foliar injury in red spruce," *BioScience*, vol. 49, no. 10, pp. 789–800, 1999.

[8] J. Holmgren, "Prediction of tree height, basal area and stem volume in forest stands using airborne laser scanningce," *Scandinavian Journal of Forest Researcht*, vol. 19, no. 6, pp. 543–553, 2004.

[9] S. G. Aracil and R. B. A. Herries, D.L, "Evaluation of an additional lidar metric in forest inventory," *Proceedings of Silvilaser*, 2015.

[10] M. J. Harper, M. A. McCarthy, R. Van Der Ree, and J. C. Fox, "Overcoming bias in ground-based surveys of hollow-bearing trees using double-sampling," *Forest Ecology and Management*, vol. 190, no. 2, pp. 291–300, 2004.

[11] L. Rayner, M. Ellis, and J. E. Taylor, "Double sampling to assess the accuracy of ground-based surveys of tree hollows in eucalypt woodlands," *Forest Ecology and Management*, vol. 36, no. 3, pp. 252–260, 2011.

[12] R. B. Smith, *Introduction to Hyperspectral Imaging.* MicroImages, 2014.

[13] W. Wanger, A. Ullrich, T. Melzer, C. Briese, and K. Kraus, "From single-pulse to ful-waveform airborne laser scanners," *ISPRS Journal of Photogrammetry and Remote Sensing*, vol. 60, pp. 100–112, 2004.

[14] A. Wehr and U. Lohr, "Airborne laser scanning - an introduction and overview," *ISPRS Journal of Photogrammerty and Remote Sensing*, vol. 54, pp. 68–82, 1999.

[15] C. Mallet and F. Bretar, "Full-waveform topographic lidar: State-of-the-art," *ISPRS Journal of Photogrametry and Remote Sensing*, vol. 64, pp. 1–16, 2009.

[16] K. Anderson, S. Hancock, M. Disney, and K. Gaston, "Is waveform worth it? a comparison of lidar approaches for vegetation and landscape characterization," *Remote Sensing in Ecology and Conservation*, 2015.

[17] A. Chauve, C. Mallet, F. Bretar, S. Durrieu, M. Deseilligny, and W. Puech, "Processing full-waveform lidar data: Modelling raw signals," *International Archives of Photogrammetry, Remote Sensing and Spatial Information Sciences*, 2007.

[18] *LAS Specification version 1.3-R1.* Bethesda, Maryland: American Society for Photogrammetry and Remote Sensing, 2010.

[19] M. Warren, *Full Waveform Upgrade.* NERC ARSF wiki, 2012.

[20] M. J. Sumnall, R. A. Hill, and S. A. Hinsley, "Comparison of small-footprint discrete return and full waveform airborne lidar data for estimating multiple forest variables," *Remote Sensing of Environment*, vol. 173, pp. 214–223, 2016.

[21] K. H. R. A. . Z. A. Lehner, H., "Consideration of laser pulse fluctuations and automatic gain control in radiometric calibration of airborne laser scanning data.," *Proceedings of 6th ISPRS Student Consortium and WG VI/5 Summer School*, 2011.

[22] I. Korpela, H. O. Ørka, H. V. Hyyppä, J., and T. Tokola, "Range and agc normalization in airborne discrete-return lidar intensity data for forest canopies," vol. 65, no. 4, pp. 369–379, 2010.

[23] M. Isenburg, *LAStools - efficient tools for LiDAR processing.* rapidlasso.

[24] M. Warren, B. Taylor, M. Grant, and J. D. Shutler, "Data processing of remorely sensed airborne hyperspectral data using the airborne processing library (apl)," *ScienceDirect, Computers and Geosciences*, vol. 64, 2014.

[25] M. Isenburg, "Pulsewaves: An open, vendor-neutral, stand-alone, las-compatible full waveform lidar standard.," 2012.

[26] A. Persson, U. Soderman, J. Topel, and S. Ahlberg, *Visualisation and Analysis of full-waveform airborne laser scanner data.* V/3 Workshop, Laser scanning 2005, 2005.

[27] M. Miltiadou, M. A. Warren, M. Grant, and M. Brown, "Alignment of hyperspectral imagery and full-waveform lidar data for visualisation and classification purposes," *The International Archives of Photogrammetry, Remote Sensing and Spatial Information Sciences*, vol. 40, no. 7, p. 1257, 2015.

[28] W. Wanger, A. Ullrich, V. Ducic, T. Maizer, and N. Studnicka, "Gaussian decompositions and calibration of a novel small-footprint full-waveform digitising airborne laser scanner," *ISPRS Journal of Photogrammetry and Remote Sensing*, vol. 60, pp. 100–112, 2006.

[29] A. Neuenschwander, L. Magruder, and M. Tyler, "Landcover classification of small-footprint full-waveform lidar data," *Jounal of Applied Remote Sensing*, vol. 3, no. 1, pp. 033544–033544.

[30] J. Reitberger, P. Krzystek, and U. Stilla, "Analysis of full waveform LiDAR data for tree species classification," *International Journal of Remote Sensing*, vol. 29, no. 5, pp. 1407–1431, 2008.

[31] A. Chauve, F. Bretar, S. Durrieu, M. Pierrot-Deseilligny, and W. Puech, "Fullanalyze: A research tool for handling, processing and analysing full-waveform lidar data," *IEEE International Geoscience and Remote Sensing Symposium*, 2009.

[32] P. Bunting, J. Armston, D. Clewley, and R. M. Lucas, "Sorted pulse data (spd) library—part ii: A processing framework for lidar data from pulsed laser systems in terrestrial environments," *Computers & Geosciences*, vol. 56, pp. 207–215, 2013.

[33] L. Cao, N. Coops, L. Innes, J. Dai, and H. Ruan, "Tree species classification in subtropical forests using small-footprint full-waveform lidar data," *International Journal of Applied Earth Observation and Geoinformation*, vol. 49, pp. 39–51, 2016.

[34] S. Hancock, K. Anderson, M. Disney, and K. J. Gaston, "Measurement of fine-spatial-resolution 3d vegetation structure with airborne waveform lidar: Calibration and validation with voxelised terrestrial lidar.," *Remote Sensing of Environment*, vol. 188, pp. 37–50, 2017.

[35] M. Miltiadou, M. Grant, M. Brown, M. Warren, and E. Carolan, "Reconstruction of a 3d polygon representation from full-wavefrom lidar data," *RSPSoc Annual Conference 2014, New Sensors for a Changing World*, 2014.

[36] R. Crippen, "Calculating the vegetation index faster," *Remote Sensing of Environment*, vol. 34, no. 1, pp. 71–73, 1990.

[37] R. N. Clark, G. A. Swayze, R. Wise, K. E. Livo, T. Hoefen, R. F. Kokaly, and S. J. Sutley, "Usgs digital spectral library splib06a," *US Geological Survey, Digital Data Series*, vol. 231, 2007.

[38] P. Hanrahan, "Ray tracing algebraic surfaces," *ACM SIGGRAPH Computer Graphics*, vol. 17, no. 3., 1983.

[39] H. Pfister, J. Hardenbergh, J. Knittel, H. Lauer, and L. Seiler, "The volumepro real-time ray-casting system," *Proceedings of the 26th annual conference on Computer graphics and interactive techniques*, pp. 251–260, 1999.

[40] J. Nickolls, I. Buck, M. Garland, and K. Skadron, "Scalable parallel programming with cuda," *Queue*, vol. 6, no. 2, pp. 40–55, 2008.

[41] C. Crassin, F. Neyret, S. Lefebvre, and E. Eisemann, "Gigavoxels: Ray-guided streaming for efficient and detailed voxel rendering," *Proceedings of the 2009 symosium on Interactive 3D graphics and games*, pp. 15–22, 2009.

[42] J. F. Blinn, *A Generalization of Algebraic Surface Drawing*, vol. 1. ACM Transactions on Graphics (TOG).

[43] A. Pasko and V. Savchenko, *Blending operations for the functionally based constructive geometry.* 1994.